Solution Conformation of an Atrial Natriuretic Peptide Variant Selective for the Type A Receptor‡

Wayne J. Fairbrother,*,§ Robert S. McDowell,‖ and Brian C. Cunningham§

Departments of Protein Engineering and Bioorganic Chemistry, Genentech, Inc., 460 Point San Bruno Boulevard, South San Francisco, California 94080-4990

Received March 7, 1994; Revised Manuscript Received May 9, 1994®

ABSTRACT: Two-dimensional NMR spectroscopy has been used to characterize the solution conformation of an atrial natriuretic peptide (ANP) variant which is selective for the human natriuretic peptide receptor A (NPR-A) relative to receptor C (NPR-C). The ANP mutant, containing six substitutions, has reduced flexibility in aqueous solution relative to wild-type ANP and allows the observation of sufficient NOE connectivities for structure determination by distance geometry and restrained molecular dynamics calculations. The solution conformation is reasonably well defined, having an average backbone atom rms deviation from the average coordinates of ~1.1 Å for residues 7–27. The stucture is consistent with available functional data and shows a spatial separation between known receptor binding determinants and residues found to be outside the hormone–receptor interface.

Atrial natriuretic peptide (ANP) is a 28-residue polypeptide hormone with regulatory roles in blood pressure, fluid, and electrolyte homeostasis; the actions of ANP are in opposition to the actions of the renin/angiotensin II/aldosterone system (Baxter et al., 1988; Laragh & Atlas, 1988; Inagami, 1989; Brenner et al., 1990; Rosenzweig & Seidman, 1991). Three distinct natriuretic peptide receptors have been described: NPR-A (Chinkers et al., 1989; Lowe et al., 1989) and NPR-B (Chang et al., 1989; Schulz et al., 1989), which are both approximately 1030-residue transmembrane guanylyl cyclases, and NPR-C (Fuller et al., 1988), which is a 496-residue transmembrane protein, also known as the clearance receptor. ANP is known to selectively stimulate the guanylyl cyclase activity of NPR-A relative to NPR-B; most of the physiological activity of ANP may be attributed to this activation (Maack, 1992). The interactions of ANP with NPR-A and with NPR-C, however, are of comparable affinity [dissociation constants are 1–2 pM, as determined for IgG:NPR-A extracellular domain and IgG:NPR-C extracellular domain fusion proteins (Bennett et al., 1991)]. NPR-C internalizes natriuretic peptides for degradation (Nussenzveig et al., 1990), hence its label as the clearance receptor, and together with kidney filtration and proteolysis (Koehn et al., 1987; Olins et al., 1987; Sonnenberg et al., 1988; Tamburini et al., 1989) appears to regulate serum ANP concentrations; the serum half-life of ANP is less than about 3 min (Espiner et al., 1985). NPR-C may also be involved in signal transduction (Hirata et al., 1989; Anand-Srivistava et al., 1990; Levin, 1993).

A number of NMR studies have been undertaken with the aim of determining the solution conformation of ANP (and ANP analogs), in order to gain some insight into its bioactive conformation. Initial studies with rat ANP (and rat ANP analogs) in both aqueous and dimethyl sulfoxide (DMSO) solutions indicated that ANP is flexible and has little or no structure (Fesik et al., 1985; Theriault et al., 1987; Gampe et al., 1988). Later studies with human ANP in DMSO solution indicated several regions having partially ordered structures (Kobayashi et al., 1988; Koyama et al., 1990). However, the overall conformation of human ANP, calculated using distance geometry methods, could not be defined from this work. Investigations of the cyclic portion (residues 7–23) of rat ANP in sodium dodecyl sulfate (SDS) micelles also revealed several regions of definable structure but failed to find a unique family of structures which satisfied the NMR-derived restraints (Olejniczak et al., 1988). However, the regions of ordered structure defined by these studies differ significantly, and it is not possible to determine which, if any, of these conformations are relevant in aqueous solution.

Recently, phage display technology has been used to develop a variant of ANP which is more than 10^5-fold selective for human NPR-A relative to NPR-C and is equipotent with wild-type ANP in stimulating NPR-A guanylyl cyclase activity (Cunningham et al., 1994). This mutant form of ANP contains six substitutions relative to wild-type human ANP (Figure 1). Of the six substitutions highlighted in Figure 1, three confer NPR-A specificity (G9T, R11S, G16R) and two enhance secreted expression (R3D, R14S). The M12L mutation was included to avoid Met oxidation, which is known to inhibit NPR-A binding (Koyama et al., 1992). Note also that the mutations result in removal of two of the five Gly residues, thereby increasing the potential for a more ordered conformation in solution.

In the present study, two-dimensional ^{1}H NMR methods have been used to investigate the solution conformation of the NPR-A-selective ANP analog (Cunningham et al., 1994). The mutant form was found to be less flexible than wild-type ANP in aqueous solution, which allowed the observation of sufficient NOE interactions for structure determination by distance geometry and restrained molecular dynamics calculations. The aqueous solution structure reported here is significantly more ordered than those previously described for wild-type ANP in DMSO solution (Kobayashi et al., 1988) or the cyclic portion of wild-type ANP in SDS micelles (Olejniczak et al., 1988). Furthermore, the reported structure is validated by its consistency with experiments that have identified sets of functionally important and unimportant residues.

‡ Coordinates have been deposited in the Brookhaven Protein Data Bank under the file name 1ANP.

* To whom correspondence should be addressed.
§ Department of Protein Engineering.
‖ Department of Bioorganic Chemistry.

® Abstract published in *Advance ACS Abstracts,* July 1, 1994.

0006-2960/94/0433-8897$04.50/0

```
                  5         10        15        20        25
WT-hANP  S L R R S S C F G G R M D R I G A Q S G L G C N S F R Y
             |             |   | |   |   |
mutant   S L D R S S C F T G S L D S I R A Q S G L G C N S F R Y
```

FIGURE 1: Sequence alignment of wild-type human ANP (top) and the NPR-A-selective ANP variant (bottom). The substituted residues are highlighted in the mutant sequence. The sequence of wild-type rat ANP differs from that of human ANP only at residue 12, which is an Ile.

METHODS

Sample Preparation. The NPR-A-selective ANP mutant was expressed in *Escherichia coli*, and the secreted peptide was purified as previously described (Cunningham et al., 1994). NMR samples were prepared by dissolving approximately 2 mg of lyophilized peptide in 0.5 mL of 90% H_2O/10% D_2O or 99.99% D_2O, to give a concentration of ~1.3 mM. The sample pH was ~3.5.

NMR Measurements. All NMR spectra were recorded on a Bruker AMX 500 spectrometer at 24 °C, unless otherwise stated. Standard pulse sequences and phase cycling were employed to record the following spectra in 90% H_2O/10% D_2O solution: COSY (Aue et al., 1975), TOCSY (Braunschweiler & Ernst, 1983; Bax & Davis, 1985), with spin-lock periods of 69 and 98 ms, and NOESY (Kumar et al., 1980; Bodenhausen et al., 1984), with a mixing time of 300 ms. In addition, the following spectra were recorded in 99.99% D_2O solution: 2QF-COSY (Rance et al., 1983), double-quantum (2Q) (Braunschweiler et al., 1984; Rance & Wright, 1986), COSY-35 (in which the COSY mixing is achieved with a 35° pulse rather than a 90° pulse as in a regular COSY), and NOESY (mixing time = 300 ms). All spectra were recorded in a phase-sensitive manner using time-proportional phase incrementation for quadrature detection in F_1 (Marion & Wüthrich, 1983). Spectra were referenced to the H_2O peak at 4.85 ppm.

Amide proton exchange with solvent was monitored at 24 °C by acquiring a series of one-dimensional proton spectra starting approximately 4 min after dissolution of a lyophilized protein sample in D_2O. Seven spectra were acquired over a total time of about 25 min. Amide proton temperature coefficients were determined from a series of COSY spectra acquired at 24, 21, 18, 15, and 12 °C.

Structure Calculations. Assigned NOE cross peaks were characterized as strong, medium, or weak, corresponding to upper bounds distance constraints of 2.7, 3.7, and 5.0 Å, respectively. All long-range NOE distance constraints were set to 5.0 Å. Lower bounds between nonbonded atoms were set to the sum of their van der Waals radii. Pseudoatom corrections were added to interproton distance constraints where necessary (Wüthrich et al., 1983); a 1.0-Å pseudoatom correction was added to all constraints involving methyl groups. No dihedral angle constraints or stereo assignments were used in the structure calculations.

Distance geometry calculations were carried out using the program DGII (Havel, 1991) within the INSIGHT II package (BIOSYM Technologies, Inc., San Diego). Following triangle bounds smoothing, random distance matrices which satisfied the triangle inequality limits were generated using metrization (Havel, 1990). Coordinates satisfying the trial distances were obtained by embedding and majorization in four dimensions. Structures were optimized by simulated annealing in four dimensions and conjugate gradient minimization in three dimensions as described by Havel (1991).

Energy refinement calculations (restrained minimization/dynamics) were carried out on the best distance geometry structures (those with the lowest total constraint violations) using the DISCOVER program (BIOSYM Technologies, Inc., San Diego). The all-atom AMBER force field (Weiner et al., 1984, 1986) was used, with a 15.0-Å cutoff for nonbonded interactions and a distance-dependent dielectric constant ($\epsilon = 4r$) to compensate for the lack of explicit solvent. Side-chain charges on Asp, Glu, Arg, and Lys residues were scaled by multiplying the default charges by 0.2 in order to reduce artifacts due to excessive charge–charge interactions. Each of the best distance geometry structures was initially minimized using 1000 steps of steepest descents minimization, followed by full conjugate gradient minimization to a maximum gradient of 0.01 kcal·mol^{-1}·Å^{-1}. The NOE distance constraints were applied using a square-well potential function (Kessler et al., 1988), with a force constant of 25 kcal·Å^{-1} throughout.

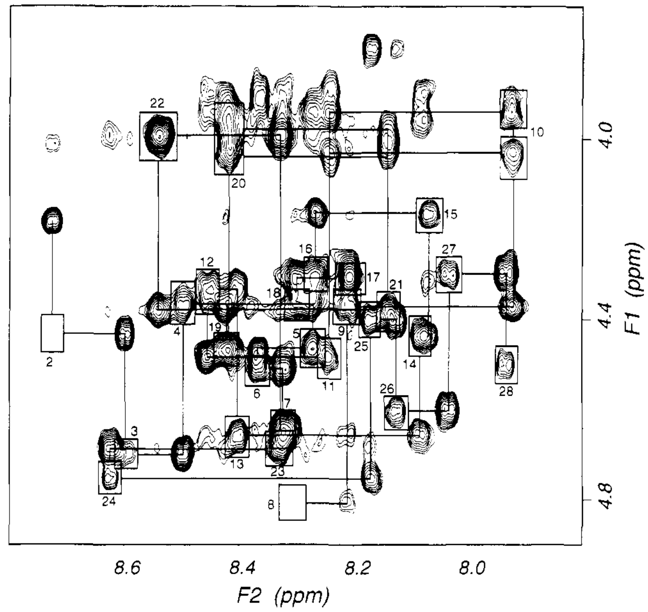

FIGURE 2: Amide–H$^\alpha$ region of a 300-ms mixing time NOESY spectrum of the NPR-A-selective ANP mutant in 90% H_2O/10% D_2O, pH 3.5, at 24 °C. Intraresidue $d_{\alpha N}$ NOE cross peaks are boxed and labeled with the residue number. The sequential $d_{\alpha N}(i,i+1)$ cross peaks are connected to the intraresidue cross peaks by the solid lines.

Each of the minimized structures was further subjected to restrained molecular dynamics. The square-well distance restraining function, with a force constant of 25 kcal·Å^{-1}, was applied throughout the dynamics. The structures were initially allowed to equilibrate at 50 K for 10 ps. The temperature of the system was then raised to 500 K by adjusting the target temperature by 25 K every 2 ps. The system was allowed to equilibrate at 500 K for 50 ps before being cooled slowly to 50 K by reducing the target temperature by 25 K every 2 ps. After a 10-ps reequilibration interval at 50 K, the structures were minimized for 1000 cycles using steepest descents, followed by conjugate gradient minimization to a maximum gradient of 0.01 kcal·mol^{-1}·Å^{-1}.

All calculations were performed on a Silicon Graphics 4D/440 computer.

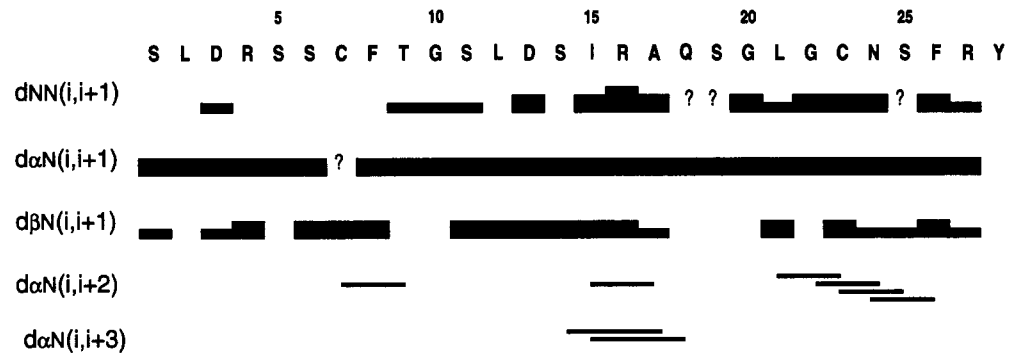

FIGURE 3: Summary of the sequential NOE connectivities observed for the NPR-A-selective ANP analog. Question marks (?) indicate that assignment of an observed cross peak is ambiguous.

Table 1: Measured $^3J_{HN\alpha}$, $^3J_{\alpha\beta}$ Amide Proton Temperature Coefficients and Proton Chemical Shifts of the NPR-A-Specific ANP Mutant at 24 °C, pH 3.5

				chemical shift (ppm)					
residue	$^3J_{HN\alpha}$	$^3J_{\alpha\beta}$	$\Delta\delta/\Delta T^a$	HN	H^α	H^β	H^γ	H^δ	H^ϵ
Ser 1					4.18	4.01*[b]			
Leu 2	6.6		6.7	8.72	4.43	1.64*	1.64		
Asp 3	7.1	6.9, 7.1	6.0	8.60	4.70	2.89, 2.81			
Arg 4	6.8	5.5, 9.3	10.5	8.50	4.37	1.92, 1.78	1.65*	3.19*	7.22
Ser 5	6.7		5.7	8.27	4.47	3.94*			
Ser 6	6.7		6.7	8.36	4.51	3.93, 3.88			
Cys 8	7.3	5.0, 8.7	6.2	8.31	4.64	3.05, 2.87			
Phe 8	7.3	6.6, 8.5	4.6	8.32	4.80	3.20, 3.05		7.29*	7.36*
Thr 9	8.0	4.0	8.5	8.21	4.37	4.26	1.22		
Gly 10				7.93	4.04, 3.94				
Ser 11	6.6		7.1	8.24	4.48	3.94, 3.88			
Leu 12	6.4	4.9, 9.7	10.8	8.46	4.33	1.73, 1.64		0.94, 0.89	
Asp 13	6.9	5.8, 7.9	5.4	8.40	4.66	2.91, 2.83			
Ser 14	6.6		5.3	8.09	4.44	3.96, 3.90			
Ile 15	6.9	8.0	8.0	8.07	4.16	1.94	1.50, 1.22 (0.93)[c]	0.89	
Arg 16	6.6	5.5, 8.5	7.1	8.27	4.30	1.86, 1.80	1.66*	3.19*	7.22
Ala 17	5.9		9.2	8.21	4.31	1.44			
Gln 18	6.9	5.4, 9.1	5.8	8.30	4.36	2.20, 2.06	2.41*		7.54, 6.90
Ser 19	6.6		9.3	8.43	4.47	3.96, 3.91			
Gly 20				8.42	4.06, 3.99				
Leu 21	6.6	4.6, 10.2	7.7	8.14	4.38	1.71, 1.65	1.69	0.95, 0.90	
Gly 22			8.8	8.54	3.99*				
Cys 23	6.8	5.4, 9.2	6.4	8.33	4.69	3.19, 2.98			
Asn 24	7.3	5.8, 7.8	8.0	8.62	4.75	2.85, 2.82		7.64, 6.99	
Ser 25	6.9		7.0	8.17	4.40	3.80*			
Phe 26	7.1	6.8, 8.6	6.1	8.13	4.60	3.07, 3.01		7.20*	7.30*
Arg 27	7.8	6.3, 8.3	6.3	8.03	4.30	1.74, 1.63	1.50*	3.16*	7.16
Tyr 28	7.8	4.9, 9.0		7.93	4.50	3.16, 2.93		7.17*	6.87*

[a] $\times 10^3$ ppm·K^{-1}. [b] Asterisks indicate degenerate proton chemical shifts. [c] Values in parentheses correspond to Ile $C^\gamma H_3$.

RESULTS

NMR Measurements. Sequential assignment of all the backbone and most of the side-chain proton resonances of the ANP hexamutant was achieved using the conventional homonuclear NOE-based assignment strategy (Billeter et al., 1982; Wüthrich, 1986). Initial spin system assignments were obtained using COSY and TOCSY spectra acquired in 90% H_2O/10% D_2O solution and 2QF-COSY and 2Q spectra acquired in D_2O solution. NOESY spectra were used to identify sequential backbone connectivities (Figure 2). A summary of the sequential NOE data is given in Figure 3, and the assignments are listed in Table 1. The observation of several weak $d_{\alpha N}(i,i+2)$ and $d_{\alpha N}(i,i+3)$ NOE connectivities (Figure 3) indicates the presence of turnlike structures in the peptide. In addition, a number of other medium- and long-range NOE cross peaks were identified in the 300-ms NOESY spectra acquired in 90% H_2O/10% D_2O or 99.99% D_2O solution (Figure 4), indicating that a significant population of structured peptide exists in aqueous solution. Figure 4B illustrates the distribution of the observed NOE connectivities on a per residue basis; a total of 267 NOEs were assigned, consisting of 117 intraresidue, 86 sequential, 33 medium-range [15 (i,i+2), 11 (i,i+3), and 7 (i,i+4)], and 31 long-range connectivities. These NOE connectivities were converted to upper bound distance constraints and used as input for the structure calculations detailed below. The intraresidue and sequential NOEs resulted in only 31 and 46 structurally useful distance constraints, respectively; the total number of structurally useful NOE distance constraints used was therefore 141.

The observation of medium- and long-range NOE connectivities clearly indicates that the ANP hexamutant is less flexible in solution than wild-type ANP; no such NOEs were observed for wild-type ANP in aqueous solution (Theriault et al. 1987; W. J. Fairbrother, unpublished results). However, other NMR parameters measured for the ANP hexamutant support the conclusion that the peptide retains a significant degree of flexibility. For instance, analysis of the H^α chemical shifts using the data smoothing protocol of Pastore and Saudek (1990) or the chemical shift index method of Wishart et al.

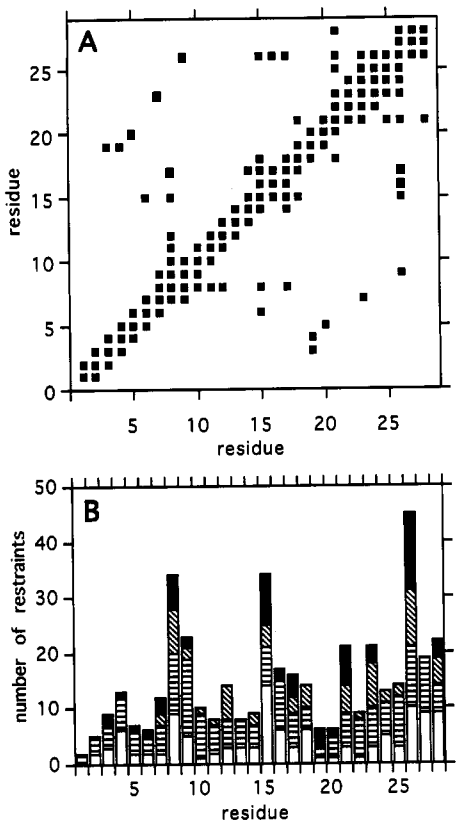

FIGURE 4: Distribution of the observed NOE connectivities in the NPR-A-selective ANP analog. (A) A diagonal plot representation of the observed NOE connectivities. A filled square indicates the presence of at least one NOE between protons in the connected residues. (B) Distribution of the NOE connectivities on a per residue basis. Open bars represent intraresidue connectivities, horizontally hatched bars represent sequential connectivities, diagonally hatched bars represent medium-range [$(i,i+2)$ to $(i,i+4)$] connectivities, and filled bars represent long-range connectivities [$>(i,i+4)$].

(1992) gives no evidence for the presence of any secondary structure. Structure is usually indicated by chemical shifts which differ from their "random coil" values, while chemical shifts with approximately random coil values are often used as evidence for flexibility.

Vicinal $^3J_{HN\alpha}$ coupling constants were determined from a COSY spectrum using the method of Kim and Prestegard (1989) (Table 1). All $^3J_{HN\alpha}$ couplings measured are between 5.9 and 8.0 Hz. These values cannot be interpreted unambiguously and could arise either from definable conformations or from averaging over many different conformations. As with the chemical shift data the $^3J_{HN\alpha}$ coupling constant data provide no evidence for stable secondary structure being present. A COSY-35 spectrum was used to measure $^3J_{\alpha\beta}$ couplings for a number of residues (Table 1). Some of these data clearly indicate unrestricted rotation about χ_1 (for example, Asp 3). The couplings measured for Thr 9, Leu 12, and Leu 21, on the other hand, indicate restricted rotation about χ_1; the magnitudes are not, however, extreme enough to allow reliable determination of the χ_1 dihedral angles. Therefore, no dihedral angle restraints were used in the structure calculations.

Amide proton exchange and resonance temperature dependence were also investigated in order to determine if any of the backbone amide protons are involved in hydrogen-bonding interactions. All the amide protons exchanged within 25 min following addition of D_2O to a lyophilized peptide sample. The half-lives for the exchanging protons were of the same order of magnitude as those expected solely on the basis of intrinsic exchange rates in unstructured peptides (Englander et al., 1979). Temperature coefficients for the amide proton chemical shifts were calculated from the temperature dependence of cross peaks in COSY spectra (Table 1). The large values found for $\Delta\delta/\Delta T$ indicate that none of the backbone amide protons are involved in stable hydrogen bonds or are otherwise protected from the solvent, consistent with the amide proton–solvent exchange results.

Structure Calculations. Distance geometry was used to calculate 100 initial structures using the set of 141 NOE-derived distance constraints discussed above; upper bounds were set to 2.7, 3.7, or 5.0 Å plus appropriate pseudoatom corrections, as discussed in Methods. From the 100 calculations, the 15 structures with the lowest final DGII error functions (less than 0.07) were chosen for further analysis. In this set of structures the largest NOE upper bound distance violation ranged from 0.16 to 0.45 Å. Figure 5A shows a superposition of the 15 best DGII structures on their mean coordinates, aligned using residues 7–27. rms differences for backbone atoms with respect to the mean coordinates for various alignments of the DGII structures are summarized in Table 2.

Each of the 15 selected DGII structures was then minimized as described in Methods, using the AMBER force field and a square-well potential function to enforce the NOE distance constraints. The largest NOE upper bound distance violation after minimization ranged from 0.05 to 0.17 Å. Five of the 15 structures (1, 5, 7, 9, and 10) had no upper bound violations greater than 0.1 Å; these structures were selected for inclusion in the final set of energy-refined structures. The 15 minimized structures were then further refined using restrained molecular dynamics. On completion of the dynamics calculations the largest NOE upper bound distance violation ranged from 0.05 to 0.24 Å. Six of the 15 structures (1, 2, 5, 6, 8, and 10) had no upper bound violations greater than 0.1 Å. These six structures, together with the five structures selected from the restrained minimization calculation, are shown in Figure 5B aligned relative to their mean coordinates using residues 7–27. Backbone rms deviations for the energy-refined ensemble of structures are listed in Table 2, and structural statistics are given in Table 3.

The conformation of the NPR-A-selective ANP analog consists of an extended, and somewhat disordered, N-terminal region (residues 1–7) with a bend in the main chain at about residue 4, a turn between residues 9–12, a helical-like turn involving residues 14–17, turns between 18–21 and 21–24, and an extended region from 24 to 27. The C-terminal Tyr residue appears disordered in the final structures. An interesting feature of the final structures is the presence of a hydrophobic cluster comprising the side chains of residues Phe 8, Leu 12, Ile 15, Leu 21, and Phe 26 (Figure 6). The final turn between residues 21–24 results in the C-terminal "tail" of the molecule being positioned such that the side chain of Phe 26 contributes to the hydrophobic core.

DISCUSSION

Wild-type ANP is inherently flexible in aqueous solution and does not adopt a definable structure, as indicated principally by the lack of medium- and long-range NOEs observed in previous NMR studies (Theriault et al., 1987; Gampe et al., 1988). We have repeated the work of Theriault et al. (1987) on wild-type rat ANP in aqueous solution, and while we observed more sequential d_{NN} NOE connectivities than in the previous study, the general conclusions were identical (W. J. Fairbrother, unpublished results). In the

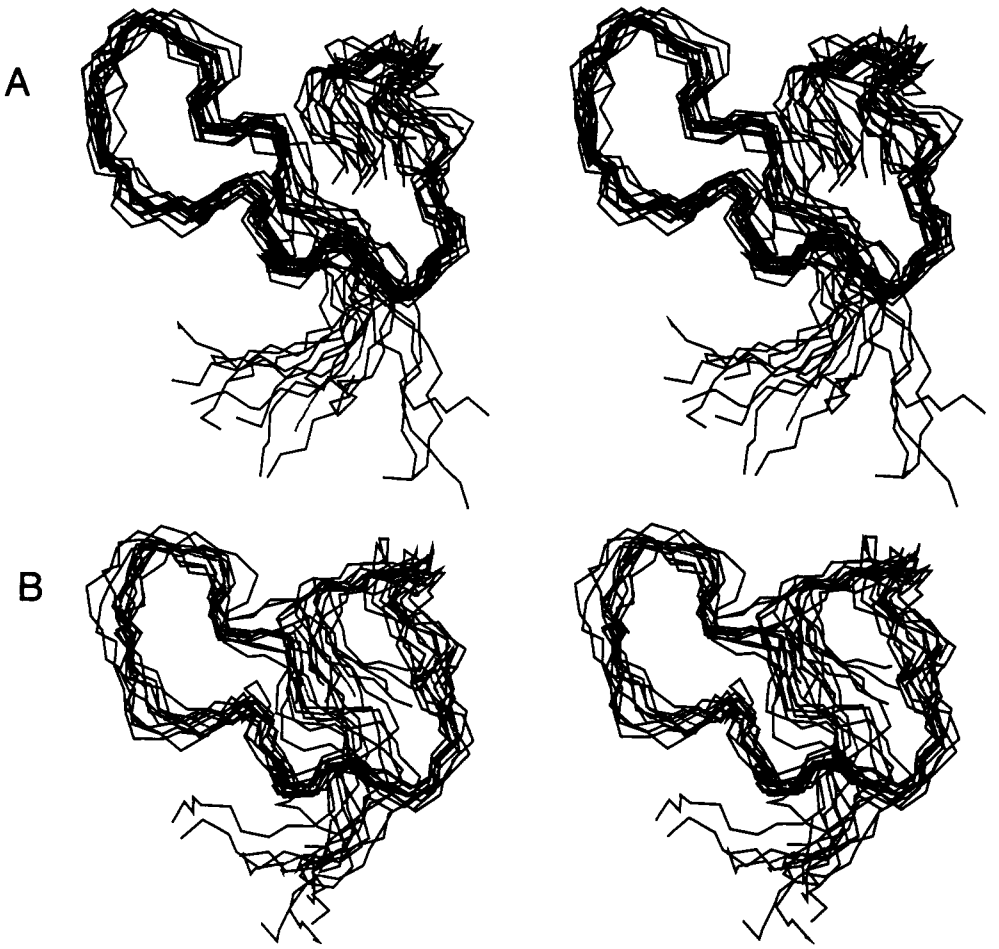

FIGURE 5: Superposition of the backbone atoms of the 15 DGII structures (A) and 11 energy-refined structures (B) of the NPR-A-selective ANP analog on their mean coordinates, aligned using residues 7–27. The mean coordinates were generated from a best fit superposition of all atoms and are shown with dotted lines. The orientation is similar to Figure 6, with the N-terminus at the bottom of each figure.

Table 2: Average rms Difference with Respect to the Mean Coordinates (Å) for the Backbone Atoms of the 15 Distance Geometry (DGII) Structures and the 11 Energy-Refined (rMin/rMD) Structures for Different Alignments of Residues[a]

aligned residues	DGII	rMin/rMD
1–28	1.68 (0.20)[b]	1.64 (0.19)
1–7	1.58 (0.34)	1.61 (0.34)
7–15	0.90 (0.11)	1.04 (0.18)
15–23	0.75 (0.15)	0.78 (0.09)
18–28	1.07 (0.26)	1.01 (0.16)
7–23	1.00 (0.14)	1.12 (0.15)
7–27	1.11 (0.13)	1.19 (0.15)

[a] The mean coordinates were calculated from a best fit superposition of all atoms. [b] Values in parentheses are standard deviations.

Table 3: Structural Statistics for the 11 Energy-Refined Structures

rms deviation from NOE distance restraints (Å) (141)[a]	0.017 (0.012)
rms deviations from idealized covalent geometry	
bonds (Å)	0.005 (0.004)
angles (deg)	1.612 (1.147)
impropers (deg)	3.833 (3.085)
energies (kcal·mol^{-1})	
F_{NOE}[b]	1.0 (0.3)
F_{bond}	3.8 (0.3)
F_{angle}	26.4 (4.8)
$F_{improper}$	1.5 (0.5)
$F_{torsion}$	24.9 (4.7)
F_{vdW}[c]	−91.6 (7.2)
F_{elec}[d]	−58.0 (7.1)
F_{total}	−92.0 (19.0)

[a] The maximum NOE distance restraint violation was 0.103 Å. [b] The final value of the square-well NOE potential was calculated with a force constant of 25 kcal·mol^{-1}. [c] F_{vdW} is the Lennard-Jones van der Waals energy calculated with the all-atom AMBER force field and a 15.0-Å cutoff. [d] F_{elec} is calculated using a distance-dependent dielectric constant ($\epsilon = 4r$).

present study we have analyzed a novel NPR-A-selective ANP analog. This hexamutant (Figure 1) is also flexible in aqueous solution, as indicated by the chemical shift dispersion, vicinal coupling constants, amide proton–solvent exchange rates, and amide proton temperature coefficients. However, unlike wild-type ANP, a number of medium- and long-range NOE connectivities were observed (Figures 3 and 4); these data could be interpreted in terms of an average solution conformation. The structures calculated in this study are not very precise (Table 2), due mainly to the inherent flexibility of this molecule; the observed NOEs are probably averaged from an ensemble of similar conformations.

Nevertheless, the average structure determined here for the ANP hexamutant is of significantly higher precision than that previously reported for wild-type human ANP in DMSO solution (Kobayashi et al., 1988). That study identified three regions of ordered structure, residues 1–7, 11–15, and 18–28. All three of these regions in the ANP hexamutant structure show significant differences relative to the conformations reported by Kobayashi et al. (1988). The N-terminal region of the ANP hexamutant studied here appears to have an extended conformation with a kink at residue 4, whereas Figure 3 of Kobayashi et al. (1988) indicates an approximately 180° chain reversal between residues 1 and 7. Conversely, Kobayashi and co-workers found residues 11–15 to populate an extended conformation not seen in the structure of the ANP

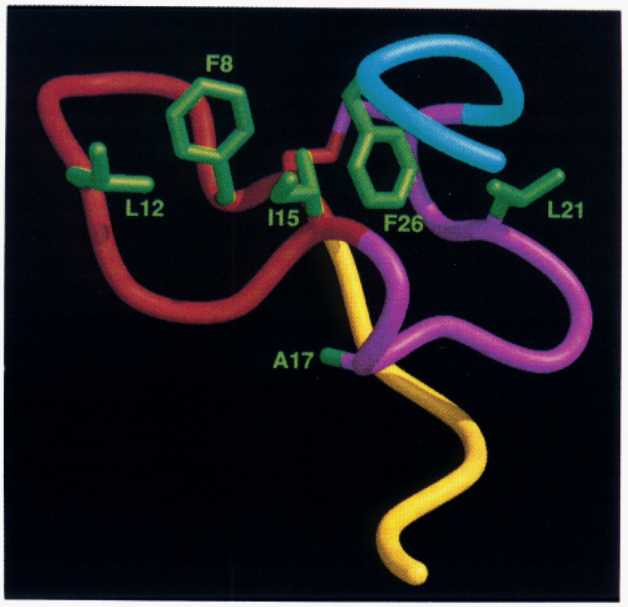

FIGURE 6: Schematic diagram of the distance geometry structure with the lowest final error, illustrating the positions of the hydrophobic side chains (except Leu 2). The main chain is colored for clarity: residues 1–6, yellow; residues 7–15, red; residues 16–23, magenta; residues 24–28, cyan.

hexamutant, in which residues 14 and 15 are the first two residues in a helical-like turn (Figures 5 and 6). It may be relevant that three of the six mutations present in the mutant peptide are located within this region (Figure 1). In the third region, residues 18–28, Kobayashi et al. identified a single turn centered around residues 22–23. While a similar turn can be identified in the ANP hexamutant, a second turn between residues 18 and 21 also exists, which was not found in the wild-type structure. A reasonable overall structure could not be determined for wild-type ANP in DMSO solution; for six structures calculated, the average pairwise rms difference for the backbone atoms was about 4.7 Å for all residues and about 3.8 Å for residues 7–23 (Kobayashi et al., 1988). The differences found between the conformations of the ANP hexamutant and wild-type ANP in aqueous and DMSO solutions, respectively, are most readily explained by the different solvent conditions under which these studies were carried out. Contributions due to the amino acid substitutions in the ANP hexamutant cannot be ruled out, however, since its structure has not been investigated in nonaqueous solvents. We note, however, that the structure determined here for the ANP hexamutant is consistent with the results of numerous structure/activity studies of ANP (see below).

Comparison of the cyclic portion of the structure of the ANP hexamutant with the structure obtained for the cyclic portion only of wild-type ANP in SDS micelles (Olejniczak et al., 1988) surprisingly reveals several similar features. Olejniczak et al. found evidence for three turn regions corresponding to residues 8–13, 14–17, and 18–21. These regions correspond closely to turns found in the present study between residues 9–12, 14–17, and 18–21, respectively, despite that fact that close to 30% of the amino acids in this region of the two peptides are different and the solvent conditions are significantly different (water compared to SDS micelles). These workers were unable, however, to determine the relative orientations of the three defined regions to give an overall conformation for the cyclic portion of wild-type ANP. From only three structures calculated the average pairwise rms difference for the backbone atoms was reported to be 3.0 Å, which may be compared with values of 1.46 ± 0.39 and 1.65 ± 0.27 Å for residues 7–23 in the DGII and energy-refined ANP hexamutant structures, respectively.

The structure of the cyclic portion of the ANP hexamutant is also similar to a model of the corresponding region of wild-type ANP that was derived from structure/activity data (Nutt et al., 1989). This model predicts turns around residues 9 and 20, which correspond closely to the turns found between residues 9–12 and 18–21, respectively, and a helical conformation for residues 12–18, corresponding to the helical-like turn observed for residues 14–17. In addition, the modeling study predicted a cluster of hydrophobic side chains from residues 8, 12, 15, and 21. As can be seen from Figure 6, these are the residues from the cyclic portion of the peptide which contribute to the hydrophobic core. The side chain of Phe 26 from the C-terminal tail of the peptide is also involved in the hydrophobic packing; this residue was not included in the earlier modeling studies. The structure reported here for the ANP hexamutant is also consistent with the stereochemical requirements observed for the residues within the cyclic portion.

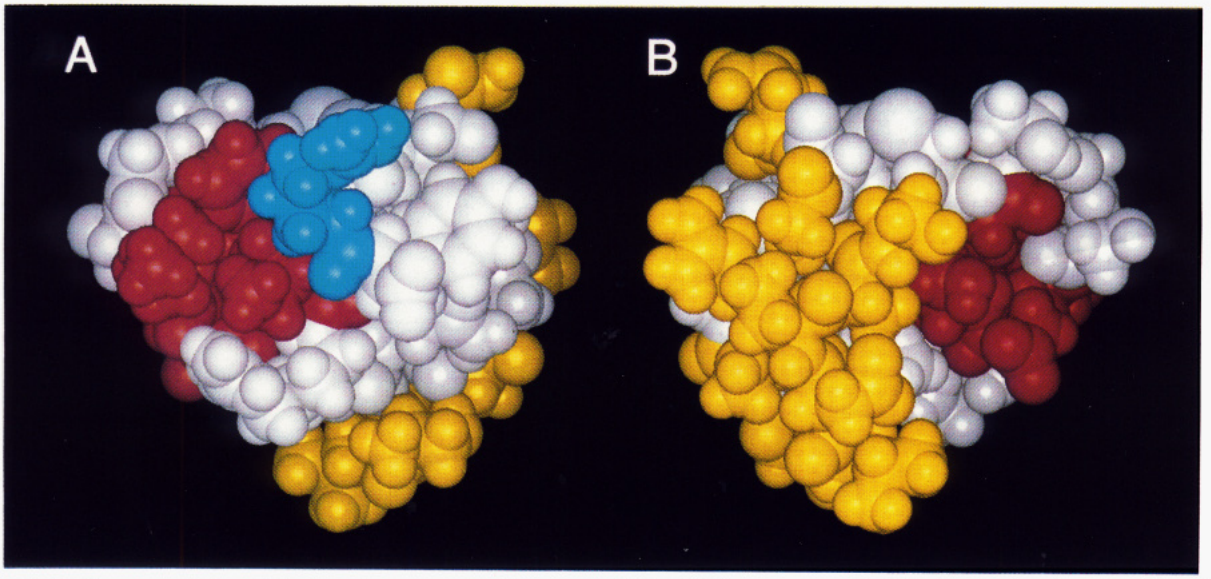

FIGURE 7: CPK representation of the lowest energy refined structure of the ANP hexamutant, highlighting the location of residues 1–6, 19, 22, and 24 in yellow, residues 8, 12, 13, 14, and 15 in red, and residue 27 in blue. (A) The orientation shown is similar to that of Figures 5 and 6. (B) Rotated about a vertical axis in the plane of the paper 180° relative to (A).

Analysis of the molecular dynamics trajectories in the present study revealed that only those residues that can functionally tolerate substitution by D-amino acids, when evaluated as inhibitors of methoxamine-induced contraction in rabbit aorta tissue (Nutt et al., 1989), explored the positive region of ϕ-space (note that no dihedral angle constraints were applied during these calculations), while those that cannot functionally tolerate substitution by D-amino acids did not (R. S. McDowell, unpublished observations). The former includes residue 9 (Gly in wild-type ANP) which has been shown to fully tolerate substitution with D-Ala, but suffers a 10-fold loss in potency on substitution with L-Ala, within the wild-type sequence of ANP (Nutt et al., 1989). The substitution G9T, present in the ANP analog studied here, is one of the mutations which confers NPR-A specificity. In the energy-refined structures this residue shows a distinct preference for a positive ϕ angle: $53 \pm 9°$ in 9 out of the 11 final structures (in the other two structures this angle is approximately $-60°$).

During the phage display selection process used in the design of the NPR-A-selective ANP hexamutant studied here (Cunningham et al., 1994), a significant number of single Cys mutations were found in positions 1–6, 19, 22, and 24. Cunningham et al. (1994) reasoned that these mutations were selected to provide a nondisruptive disulfide partner for the otherwise unpaired Cys 201 in the ANP–gene III fusion protein produced during the phage display. They further hypothesized that these mutations identify positions where disulfide bonds can form without perturbing NPR-A binding, suggesting that the substituted residues do not become buried within the hormone–receptor interface. Figure 7 highlights in yellow the location of these residues in the lowest energy-refined structure of the ANP hexamutant. In Figure 7 it can be seen that these residues form a surface on one side of the molecule; this region of ANP presumably does not interact with NPR-A. Also apparent from Figure 7 is that this region is distinct from a number of residues which have been implicated from alanine-scanning mutagenesis (Cunningham and Li, data to be published), and other previous structure/activity studies, as being important for activity (residues 8, 12, 13, 14, and 15); the red region contains residues thought to be involved in the hormone–receptor complex interface.

Another feature of the ANP hexamutant structure which correlates with previous structure/activity results is the positioning of the side chain of Arg 27 in proximity of the hydrophobic side chains of Phe 8, Leu 12, and Ile 15 (Figure 7). Several groups have suggested that a guanidine moiety, which may be supplied by either the N- or C-terminal tail sections, is important for activity (Fok et al., 1985; Brady et al., 1990; Nutt et al., 1990; von Geldern et al., 1992). From molecular modeling studies, similar to those applied to the cyclic portion of ANP, it was suggested that the C-terminal tail folds back to place the Arg 27 side chain near the critical hydrophobic residues of the cyclic core. This appears to be the case in the ANP hexamutant structure (Figure 7), although the precise conformation of the Arg 27 side chain could not be determined and is probably disordered in solution. An explanation for why the guanidine moiety may be supplied from either the N- or C-terminal tail sections (Nutt et al., 1990) is not readily apparent from the ANP hexamutant structure.

The conformation of the NPR-A-selective ANP hexamutant reported here is the most detailed structural picture of an ANP analog to date. It remains unknown, however, how this structure is related to the receptor-bound conformation of ANP. The results of a number of functional studies are compatible with this model and suggest that it may represent a conformation which is similar to the receptor-bound structure. The structure reported here will be useful in the design of further analogs to test this hypothesis. It is expected that the results from analyzing new analogs based on the ANP hexamutant structure will further our understanding of the hormone–receptor interaction and aid in the design of ANP-related therapeutics.

ACKNOWLEDGMENT

We thank Drs. David Lowe (Department of Molecular Biology, Genentech, Inc.) and Nicholas Skelton (Department of Protein Engineering, Genentech, Inc.) for many valuable discussions.

REFERENCES

Anand-Srivistava, M. B., Sairam, M. R., & Cantin, M. (1990) *J. Biol. Chem. 265*, 8566–8572.

Aue, W. P., Bartholdi, E., & Ernst, R. R. (1975) *J. Chem. Phys. 64*, 2229–2246.

Bax, A., & Davis, D. G. (1985) *J. Magn. Reson. 65*, 355–360.

Baxter, J. D., Lewicki, J. A., & Gardner, D. G. (1988) *Bio/Technology 6*, 529–543.

Bennett, B. D., Bennett, G. L., Vitangcol, R. V., Jewett, J. R. S., Burnier, J., Henzel, W., & Lowe, D. G. (1991) *J. Biol. Chem. 266*, 23060–23067.

Billeter, M., Braun, W., & Wüthrich, K. (1982) *J. Mol. Biol. 155*, 321–346.

Bodenhausen, G., Kogler, H., & Ernst, R. R. (1984) *J. Magn. Reson. 58*, 370–388.

Brady, S. F., Ciccarone, T. M., Williams, T. M., Veber, D. F., & Nutt, R. F. (1990) in *Peptides: Chemistry, Structure and Biology* (Rivier, J. E., & Marshall, G. R., Eds.) pp 598–599, ESCOM, Leiden, The Netherlands.

Braunschweiler, L., & Ernst, R. R. (1983) *J. Magn. Reson. 53*, 521–528.

Braunschweiler, L., Bodenhausen, G., & Ernst, R. R. (1984) *Mol. Phys. 48*, 535–560.

Brenner, B. M., Ballerman, M. E., Gunning, M. E., & Zeidel, M. L. (1990) *Physiol. Rev. 70*, 665–699.

Chang, M.-S., Lowe, D. G., Lewis, M., Hellmiss, R., Chen, E., & Goeddel, D. V. (1989) *Nature 341*, 68–72.

Chinkers, M., Garbers, D. L., Chang, M.-S., Lowe, D. G., Chin, H., Goeddel, D. V., & Schulz, S. (1989) *Nature 338*, 78–83.

Cunningham, B. C., Lowe, D. G., Li, B., Bennett, B. D., & Wells, J. A. (1994) *EMBO J.* (in press).

Englander, J. J., Calhoun, D. B., & Englander, S. W. (1979) *Anal. Biochem. 92*, 517–524.

Espiner, E. A., Crozier, I. G., Nicholls, M. G., Cuneo, R., Yandle, T. G., & Ikram, H. (1985) *Lancet 2*, 398–399.

Fesik, S. W., Holleman, W. H., & Perun, T. J. (1985) *Biochem. Biophys. Res. Commun. 131*, 517–523.

Fok, K. F., Tjoeng, F. S., Houbion, J. A., Spear, K. L., Nugent, S. T., Eubanks, S. R., Zupec, M. E., Olins, G. M., Blehm, D. J., & Adams, S. P. (1985) in *Peptides: Structure and Function* (Deber, C. M., Hruby, V. J., & Kopple, K. D., Eds.) pp 953–956, Pierce Chemical Co., Rockford, IL.

Fuller, F., Porter, J. G., Arfsten, A., Miller, J., Schilling, J. W., Scarborough, R. M., Lewicki, J. A., & Schenk, D. B. (1988) *J. Biol. Chem. 263*, 9395–9401.

Gampe, R. T., Jr., Connolly, P. J., Rockway, T., & Fesik, S. W. (1988) *Biopolymers 27*, 313–321.

Havel, T. F. (1990) *Biopolymers 29*, 1565–1585.

Havel, T. F. (1991) *Prog. Biophys. Mol. Biol. 56*, 43–78.

Hirata, M., Chang, C.-H., & Murad, F. (1989) *Biochim. Biophys. Acta 1010*, 346–351.

Inagami, T. (1989) *J. Biol. Chem. 264*, 3043–3046.

Kessler, H., Griesinger, C., Lautz, J., Müller, A., van Gunsteren, W. F., & Berendsen, H. J. C. (1988) *J. Am. Chem. Soc. 110*, 3393–3396.
Kim, Y., & Prestegard, J. H. (1989) *J. Magn. Reson. 84*, 9–13.
Kobayashi, Y., Ohkubo, T., Kyogoku, Y., Koyama, S., Kobayashi, M., & Go, N. (1988) *J. Biochem. 104*, 322–325.
Koehn, J. A., Norman, J. A., Jones, B. N., LeSoeur, L., Sakane, Y., & Ghai, R. D. (1987) *J. Biol. Chem. 262*, 11623–11627.
Koyama, S., Kobayashi, Y., Ohkubo, T., Kyogoku, Y., Sato, A., Kobayashi, M., & Go, N. (1990) *Protein Eng. 3*, 393–402.
Koyama, S., Terai, T., Inoue, T., Inomata, K., Tamura, K., Kobayashi, Y., Kyogoku, Y., & Kobayashi, M. (1992) *Eur. J. Biochem. 203*, 425–432.
Kumar, A., Ernst, R. R., & Wüthrich, K. (1980) *Biochem. Biophys. Res. Commun. 95*, 1–6.
Laragh, J. H., & Atlas, S. A. (1988) *Kidney Int. 34*, S64–S71.
Levin, E. R. (1993) *Am. J. Physiol. 264*, E483–E489.
Lowe, D. G., Chang, M.-S., Hellmiss, R., Chen, E., Singh, S., Garbers, D. L., & Goeddel, D. V. (1989) *EMBO J. 8*, 1377–1384.
Maack, T. (1992) *Annu. Rev. Physiol. 54*, 11–27.
Marion, D., & Wüthrich, K. (1983) *Biochem. Biophys. Res. Commun. 113*, 967–974.
Nussenzveig, D. R., Lewicki, J. A., & Maack, T. (1990) *J. Biol. Chem. 265*, 20952–20958.
Nutt, R. F., Brady, S. F., Lyle, T. A., Ciccarone, T. M., Colton, C. D., Paleveda, W. J., Williams, T. M., Smith, G. M., Winquist, R. J., & Veber, D. F. (1989) in *Synthetic Peptides: Approaches to Biological Problems* (Tam, J. P., & Kaiser, E. T., Eds.) pp 267–279, Alan R. Liss, Inc., New York.
Nutt, R. F., Ciccarone, T. M., Brady, S. F., Colton, C. D., Paleveda, W. J., Lyle, T. A., Williams, T. M., Veber, D. F., Wallace, A., & Winquist, R. J. (1990) in *Peptides: Chemistry, Structure and Biology* (Rivier, J. E., & Marshall, G. R., Eds.) pp 444–446, ESCOM, Leiden, The Netherlands.
Olejniczak, E. T., Gampe, R. T., Jr., Rockway, T. W., & Fesik, S. W. (1988) *Biochemistry 27*, 7124–7131.
Olins, G. M., Spear, K. L., Siegel, N. R., & Zurcher-Neely, H. A. (1987) *Biochim. Biophys. Acta 901*, 97–100.
Pastore, A., & Saudek, V. (1990) *J. Magn. Reson. 90*, 165–176.
Rance, M., & Wright, P. E. (1986) *J. Magn. Reson. 66*, 372–378.
Rance, M., Sørensen, O. W., Bodenhausen, G., Wagner, G., Ernst, R. R., & Wüthrich, K. (1983) *Biochem. Biophys. Res. Commun. 117*, 479–485.
Rosenzweig, A., & Seidman, C. E. (1991) *Annu. Rev. Biochem. 60*, 229–255.
Schulz, S., Singh, S., Bellet, R. A., Singh, G., Tubb, D. J., Chin, H., & Garbers, D. L. (1989) *Cell 58*, 1155–1162.
Sonnenberg, J. L., Sakane, Y., Jeng, A. Y., Koehn, J. A., Ansell, J. A., Wennogle, L. P., & Ghai, R. D. (1988) *Peptides 9*, 173–180.
Tamburini, P. P., Koehn, J. A., Gilligan, J. P., Charles, D., Palmesino, R. A., Sharif, R., McMartin, C., Erion, M. D., & Miller, M. J. S. (1989) *J. Pharmacol. Exp. Ther. 251*, 956–961.
Theriault, Y., Boulanger, Y., Weber, P. L., & Reid, B. R. (1987) *Biopolymers 26*, 1075–1086.
von Geldern, T. W., Rockway, T. W., Davidsen, S. K., Budzik, G. P., Bush, E. N., Chu-Moyer, M. Y., Devine, E. M., Jr., Holleman, W. H., Johnson, M. C., Lucas, S. D., Pollock, D. M., Smital, J. M., Thomas, A. M., & Opgenorth, T. J. (1992) *J. Med. Chem. 35*, 808–816.
Weiner, S. J., Kollman, P. A., Case, D. A., Singh, U. C., Ghio, C., Alagona, G. S., Profeta, J., & Weiner, P. (1984) *J. Am. Chem. Soc. 106*, 765–784.
Weiner, S. J., Kollman, P. A., Nguyen, D. T., & Case, D. A. (1986) *J. Comput. Chem. 7*, 230–252.
Wishart, D. S., Sykes, B. D., & Richards, F. M. (1992) *Biochemistry 31*, 1647–1651.
Wüthrich, K. (1986) *NMR of Proteins and Nucleic Acids*, John Wiley & Sons, Inc., New York.
Wüthrich, K., Billeter, M., & Braun, W. (1983) *J. Mol. Biol. 169*, 949–961.